Indian Journal of Engineering & Materials Sciences
Vol. 31, December 2024, pp. 826-842
DOI: 10.56042/ijems.v31i6.10650

Bidirectional converter with spike suppressed switching and optimized neuro restrictive steady-state controller for hybrid AC/DC microgrid

Putchakayala Yanna Reddy*& Lalit Chandra Saikia

Department of Electrical Engineering, National Institute of Technology (NIT), Silchar, Assam 788010, India

Received: 24 April 2024; accepted: 03 September 2024

A bidirectional converter (BC) is the core of a hybrid AC/DC microgrid that connects the AC and DC subgrid. However, existing hybrid AC-DC converter technologies continue to have major drawbacks and obstacles including high switching loss and stability issues. Hence a novel,Bidirectional Converter with Spike Suppressed Switching and Optimized Neuro Restrictive Steady-State Controller has been proposed to reduce switching loss and improve the steady-state performance of the microgrid. The existing converter-controlling methods fail to account for parasitic effects that impact multi-component interactions, specifically magnetic coupling during power conversion. To overcome this issue a novel Spike Suppressed Switching Circuit has been proposed, which uses a Transient Voltage Suppresser Diode (TVSD) and Field Decoupler to reduce switching loss during converter operation. The Synergic TVSD has effectively absorbed voltage spikes and reduced the extreme voltage damage to converter components. The Dualistic Field Decoupler, which consists of the Twin Ultra-Fast Recovering Diode (TUFRD) and the Mid-Snubber unit, has reduced magnetic coupling between inductors and transformers, thus lowering eddy current production. Moreover, the wind-up effect has accumulated errors in integral terms, which leads to an overshoot or a protracted settling period when the system has returned to the operational range. Therefore, an Optimized Neuro Restrictive Integration Regulator has been proposed, in which the Saturation Attending Freezing Algorithm with an optimized RBFN (Radial Basis Function Network) is used to reduce the wind-up effect and enhance the steady-state performance of the Hybrid AC/DC microgrid. The results obtained from the proposed model have a low switching loss, high efficiency, and low error.

Keywords: Dualistic field decoupler, Radial basis function network, Saturation attentive freezing, Saturation attentive freezing algorithm, Transient voltage suppressor diode

1 Introduction

A hybrid AC/DC microgrid combines direct current (DC) and alternating current (AC) technology to produce a more durable and effective power infrastructure. It is a modern, adaptable energy distribution system and this integrated strategy enables the best-localized use of various distributed energy resources (DERs) and energy storage technologies. A crucial component for ensuring smooth coordination, stability, and ideal energy management across the interconnected AC and DC components is the control of such hybrid microgrids. Complex algorithms are used in hybrid AC/DC microgrid control systems to manage energy flow, balance supply and demand, and keep voltage and frequency levels stable. These solutions must solve many issues, including the conversion of power between AC and DC, bidirectional power flow, smooth mode switching, and the optimization of energy dispatch based on real-time conditions. Higher electronics converters and output power filters are required for the connection of Renewable Energy Resources (RERs) to the utility main grid. The power converter enables the grid and RES to exchange electricity in a proper, secure, and dependable manner. Smart networks (SGs), which depend on the ability to transmit data and move power in both directions, emerged from traditional power networks[1-4].

The correct distribution, conversion, and utilization of energy inside the microgrid depend on effective power flow regulation. Managing the bidirectional flow of energy, controlling the power flow between the AC and DC sides, and reducing conversion-related losses are all necessary to achieve this. Regulation of Voltage and Frequency: The proper operation of AC networks depends on constant voltage and frequency levels. When switching between AC and DC modes or incorporating variable renewable energy sources, control algorithms must

*Corresponding author (E-mail: yannareddy.p@gmail.com)

keep an eye on and make adjustments to these parameters to keep the system stable. To use these methods, the converter's AC and DC sides must be kept at the correct voltage and current levels. It is usual practice to control these parameters and guarantee stable and consistent power flow using proportional-integral (PI) controllers. Maximum Power Point Tracking (MPPT) techniques are used to get the most power possible out of integrated renewable energy sources like solar panels. This entails modifying the converter's operating point to correspond to the source's ideal power output. Optimizing energy distribution depending on current conditions is the goal of advanced control systems. These methods decide when and how much electricity should be delivered or stored by taking into account variables including demand, energy pricing, and the condition of energy storage systems [5-8].

In hybrid microgrids, load, generation, and the state of the grid connection all fluctuate quickly. While avoiding voltage spikes, frequency aberrations, and power imbalances, control approaches must quickly respond to these dynamic alterations. It is difficult to maintain stability in a hybrid microgrid with bidirectional power flow. Complex control methods are needed because of the potential voltage and frequency instability caused by interactions between AC and DC systems. For seamless power exchange, it is essential to make sure that the AC and DC networks are properly synchronized. Power quality problems and inefficiencies can be caused by misaligned frequencies or phases. In the microgrid, bidirectional converters frequently need to interface with other parts and controllers. The stability of the entire system depends on the establishment of dependable communication and coordination protocols. Harmonics and electromagnetic interference can enter the microgrid through bidirectional converters. To guarantee electricity quality and avoid disruptions, filtering and mitigation strategies are required. Switching losses happen when semiconductor devices switch between the on-state and the off-state. The duration of the devices' state transitions and the corresponding voltage and current waveforms are to blame for these losses[9–12].

Switching losses rise when switching frequencies rise because more transitions occur regularly. Higher frequencies might additionally be capable of improving dynamic response and harmonic mitigation. The switching losses in a converter are influenced by the properties of the semiconductor devices employed in it. Because more energy is being switched at higher voltage and current levels, switching losses are typically higher. Traditional control methods that rely on exact system model parameters may encounter several issues when exposed to strong shocks. To do this, robust system operations utilizing non-model-based methods such as model predictive controllers (MPC), artificial neural networks (ANNs), and fuzzy logic are described. In this regard, many artificial and deep neural network-based intelligent elements are applied for increased performance, such as managing DC-DC converters with ANNs to deliver a constant output voltage. In microgrid control scenarios, optimal power dispatch, battery charging and discharging rates, and load demand forecasts have all been predicted using feed forward neural networks (FNNs)[13–15]. In microgrids, managing switching losses, steady-state performance, dynamic changes, and balancing numerous energy sources provide problems for bidirectional control techniques. Therefore, a novel controlling strategy and deep learning-based approaches are required to address these problems by learning patterns, optimizing switching strategies, anticipating stability problems, and adapting to changing conditions, leading to more effective, resilient, and adaptive microgrid management systems.

The main contribution of this paper is as follows:

- To address the flaws of the existing AC/DC microgrid's bidirectional converter control approaches, a novel Bidirectional Converter with Spike Suppressed Switching and Optimized Neuro Restrictive Steady-State Controller is proposed.
- To reduce the switching loss, a novel Spike Suppressed Switching Circuit is introduced, in which Synergic TVSD is utilized to prevent an excessive voltage from external load variations, and a Dualistic Field Decoupler is utilized to avoid magnetic coupling inductors and transformer and reduce the eddy current formation.
- To regulate the steady-state performance of the microgrid componentsa novel Optimized Neuro Restrictive Integration Regulator is proposed, which reduces the impact of the wind-up effect by preventing error growth in the integration section and enhancing steady-state performance.

2 Material and Methods

Silveira *et al*[16] presented a Power Management System for a hybrid microgrid that worked in both disconnected and connected to the grid modes. The modified interlinking converters consisted of an interlinking converter (ILC), which operated under the operation mode, and a two-stage interlinking converter-energy storage device (TSILC-ESD). The TSILC-ESD served as a grid-supporting unit for both microgrids while the ILC served as a grid-forming unit for the DC microgrid in grid-connected mode.In this case, the BMS's activation of the TSILC-ESD caused it to be disabled. While the ILC established the AC microgrid, the TSILC-ESD independently formed the DC microgrid. The AC microgrid received additional support from the TSILC-ESD. The BMS used a load or source selectivity depending on the SoC conditions to maintain the formation of both grids, however, this article did not address data loss in a real communication system within the microgrid, which results in control problems in experimental test benches.

Ortiz *et al*[17] presented an AC/DC HMG benchmark that was based on the IEEE 14-node test feeder. Photovoltaic energy resources were taken into consideration when selecting renewable energy sources rather than wind energy resources. This AC/DC HMG benchmark featured a one-line schematic and all necessary details for the 13,8 kV primary system and the 0,22 kV secondary system. For the suggested experiment, two scenarios minimal and maximal power demands—were used. There was a measurement module on each bus.By simulating observations related to power quality indices like current and voltage total harmonic distortion (THDV and THDI), power line losses and power factor were calculated. However, it was challenging to control the fast dynamics and quick reactions of the dispersed energy supplies.

Hang Yu *et al*[18] proposed a scalable, adaptive hybrid AC/DC microgrid clustering system and decentralized control methodology. The multi-stage, integrated ILC known as ENU was the key component that links the AC, DC sub-grid, and external power grid to create the unified microgrid cluster. The reconfigurable topologies of ENUs enable islanded DC interconnection and grid-connected AC connectivity of microgrids using the same converter modules, hence decreasing the number of conversion units and the system's cost, weight, and size.In the event of an island, adaptive and autonomous power coordination across microgrids was achieved while taking DC line voltage and cluster capacity restrictions into account. However, this architecture does not take into account the dispersed communication's ability to spread economic power.

Tushar Kanti Roy *et al*[19] presented a robust backstepping control strategy to ensure the dynamic stability of the hybrid AC/DC microgrid. The Lyapunov control functions were theoretically used to gauge dynamic stability by searching for decreases in the pace at which the energy corresponding to various states was changing. The external disturbances were modeled in terms of parametric uncertainties, modeling errors, and external disturbances for which the control signal was established by applying adequate constraints, providing dynamic stability in every circumstance. Even if the developed controllers were used for a specific hybrid AC/DC microgrid structure, the developed control method was able to be applied to any source (such as fuel cells, diesel generators, etc.) whose models were represented by the set of differential equations. However, because this strategy does not take parametric ambiguity factors into account, the resilience against parametric uncertainty has not been validated.

Tae-Gyu Kim *et al*[20] proposed an EMS for a hybrid AC/DC microgrid based on artificial neural networks (ANN). The microgrid was powered by the ANN, which consists of a two-step process that outputs the operating mode and charges and discharges the ESS. An ESS, a solar converter, a wind converter, and an interlinking converter to connect with the AC distribution system make up the microgrid. In grid-connected mode, the ILC (Interlinking Converter) regulates both the current of the AC-distributed system and the voltage of the DC microgrid.The PV and WT (Wind Turbine) converters controlled the maximum power point tracking (MPPT). The mode selection made by the ANN determined each converter's control technique. The ANN is, however, problematically sensitive to changes in noise and data quality, which are influenced by outside influences.

Jasim *et al*[21] developed a distributed hybrid DC/AC Microgrid (MG) current controller based on an Infinite Impulse Response (IIR) filter and proportional-resonant (PR) current theory. This

controller tracked the Maximum Power Point (MPP) while controlling the inverter's output current using an adaptive neuro-fuzzy inference system (ANFIS) that was trained using particle swarm optimization (PSO). The most power may be harvested from solar Photovoltaic (PV) systems based on boost converters and inverters by using a hybrid ANFIS-PSO that is quick and oscillation-free. High gain at the grid frequency was achieved with the proposed PR controller while harmonics were canceled. The PR controller has several advantages, including quick reference signal tracking, grid frequency drift adaptation, straightforward system design, and the absence of steady-state error. However, due to the computational cost of the PSO technique, this strategy cannot be applied in large-scale microgrids with several DERs and sophisticated control strategies.

Lv *et al*[22] proposed an approach to create a two-stage bidirectional power converter (BPC) with adjustable inertia to improve the dynamic performance of the hybrid power system. In more detail, the first stage of the BPC simulates the inertia frequency response in the AC bus and is operated as a virtual synchronous generator to support the AC subgrid. The second stage regulates the BPC's internal capacitor to implement programmable inertia for the DC subgrid and enhance the DC bus voltage response. In addition, the terminal voltage of the integrated capacitor was also limited to guarantee the BPC's proper operation. Power converters are able to respond to grid changes fast, but because of their longer response time and precision, they do not precisely mimic the inertia response of rotating generators.

Bandla *et al*[23] presented a decentralized virtual inertial control system for hybrid energy storage systems (HESS) and hybrid AC-DC microgrids to function collectively as a synchronous generator. The suggested control scheme makes use of a high power density storage device, such as an ultra-capacitor integrated into the DC side, to function as rotor mass and create the virtual inertia required by the power system, and a battery to act as a virtual governor to fill the steady state power deficit during islanded and community connected modes of operation. This ensured efficient power distribution among the hybrid AC-DC microgrids. Through PHIL simulation of numerous hybrid AC-DC microgrids operating in utility, community, and islanded modes, the effectiveness of the proposed VSG method was confirmed. The hybrid AC-DC microgrid exhibits a lack of transient and steady-state response during community-connected and islanded modes of operation.

Abulanwar *et al*[24] proposed a hybrid AC/DC microgrid's adaptive synergistic control technique and investigated under various operating circumstances. The proposed synergistic control technique, which was based on the voltage behavior of supercapacitors, guarantees that power transfer between renewable resources and storage media takes into account their operating restrictions and also allows the hydrogen management system to operate more cost-effectively and for longer periods. More crucially, adaptive management of the grid-side converter reduced the impact of rapid variations in load on the AC bus voltage under a wide range of changes in grid impedance, hence enhancing the durability of the microgrid when in load-shedding mode. Additionally, the grid-side converter's capacity to successfully tolerate high transient currents was increased when super fault current limiters were supporting AC bus voltage during various failures. This allows the microgrid to be linked without interruptions even during fault scenarios.

Yang *et al*[25] proposed a three-state dual-inductor bi-directional converter architecture as a solution to the current spike issues. The suggested topology was also given an adaptive control system. A suggested adaptive current feedback control approach based on the valley voltage loop was used to drive the power switches in the control technique, while the load current waveform was used to drive the inductor branch selection switches. The stability of the power supply system tends to be successfully ensured thanks to the three-state dual-inductor bi-directional converter suggested in this study, which is able to manage the bus current spike. The circuit's dependability is impacted by the high pulse load frequency of the topology, which causes a large current peak and a protracted transient adjustment time, especially when the pulse load frequency varies.

Reddy *et al*[26] provided synchronization and discrimination between positive and negative sequences in discrete blocks, a unique Synchronous Reference Frame Phase-Locked Loop (SRF-PLL) with a Self-curing decoupling network is introduced. In order to remove fluctuations in grid variables on both the AC and DC sides, a new multi-loop

controller featuring a central Deep Belief Network (DBN) and fuzzy controller, called the Switched Tuned Arm Filter (STAF) and Variable Voltage Stabilization Compensator (VVSC), was introduced. It used tuned circuits to suppress higher-order harmonics using an STAF Multi-loop controller. Additionally, an AC/dc converter receives a control signal from a central DBN equipped with a fuzzy controller to manage power transmission. However, with the increasing need for eco-friendly and economical energy solutions, DC microgrids have become a ray of hope.

Overall from this literature survey, it is understood that[16] has control issues in experimental test benches,[17] has difficulties in handling quick dynamics of the dispersed energy resources,[18] the economic power dispatching with distributed communication has not been considered,[19] does not consider parametric ambiguity factors,[20] result was affected due to the noise in the dynamic data and[21] involved computational burden and affected the performance of microgrid,[22] they do not precisely mimic the inertia response of rotating generators,[23] exhibits a lack of transient and steady-state response,[24] there is a need for reliable and uninterrupted operation of a microgrid during fault scenarios in[25] circuit's dependability is impacted by the high pulse load frequency of the topology, which causes a large current peak, and in[26] with the increasing need for eco-friendly and economical energy solutions, DC microgrids have become a ray of hope. Hence, there is a need for a novel approach to eliminate all these issues and improve the steady state functioning of hybrid microgrids.

2.1 Bidirectional converter with spike suppressed switching and optimized neuro restrictive steady-state controller

The integration of renewable energy sources and energy storage systems in microgrids has gained significant attention due to their potential to improve energy efficiency and environmental sustainability. The hybrid AC-DC converter has become an essential part of microgrids because it allows for bidirectional power flow and enables the smooth integration of various power sources and loads. However, there are still significant drawbacks and difficulties with the existing hybrid AC-DC converter technologies such as high switching loss and stability issues. Hence a novel Bidirectional Converter with Spike Suppressed Switching and Optimized Neuro Restrictive Steady-State Controller is introduced, which overcomes the limitations of the existing Bidirectional Converter Controlling Approaches by reducing the switching loss and improving the steady-state performance of the microgrid. Bidirectional converter circuit designs have parasitic features like stray inductances and capacitances that cause voltage spikes and ringing during switching events, which increases switching losses. Existing converter-controlling approaches overlook parasitic effects on multi-component interaction, leading to magnetic coupling between inductors and transformers during the sudden release of previously stored energy leading to leakage inductance and eddy current losses and switching losses, affecting the efficiency and performance of power converters. Hence a novel Spike Suppressed Switching Circuit is introduced, to reduce the switching loss in the converter by using Synergic TVSD and a Dualistic Field Decoupler. The Synergic TVSD (Transient Voltage Suppressor Diode) is comprised of two parallel TVS diodes connected to the primary buses, both on the AC and DC sides. It provides a low-impedance path for the sudden transient current to flow through itself and absorbs the voltage spike. Consequently, this prevents excessive voltage from external load variations from passing into the protected components of the converter circuit. Also, the inductor and transformer are connected in parallel with a Dualistic Field Decoupler, consisting of a Twin Ultra-Fast Recovering Diode (TUFRD) and a Mid-Snubber unit to avoid magnetic coupling. The TUFRDs are designed to have low junction capacitance and promote quicker recombination of charge carriers, which allows for faster switching of current flow in alternate paths in either direction. To further protect the circuit, a Mid-Snubber unit is included, which consists of a resistor and capacitor connected in series and placed in a center-parallel arrangement to the TUFRDs. The capacitor in this unit serves as an additional protection, which absorbs any excess rapid spikes in magnetic field variation caused by sudden voltage barbs. This helps to avoid magnetic coupling between the inductors and transformer and reduces eddy current formation and energy loss due to heating. Hence, this novel Spike Suppressed Switching Circuit improves the switching speed, reduces switching loss, and considers the parasitic effect on multiple component interaction thereby eliminating magnetic coupling and improving the converter’s performance.

Furthermore, in previous techniques, PI controllers are often designed to accomplish steady-state regulation, but they have a delayed reaction to disturbances, particularly in systems with high dynamics, such as those containing energy storage and electronic converters. In control systems, the wind-up effect causes problems because the integral term keeps accumulating errors even when the control signal has reached its limit. This leads to an overshoot or a long settling time when the system returns to its operating range. Additionally, existing Deep Learning-based controllers do not address controlled integration of errors, which can result in stability issues and damage to the system or its components. Therefore, a novel Optimized Neuro Restrictive Integration Regulator is introduced, wherea Restrictive Integration namely, Saturation Attentive Freezing algorithm is introduced with optimized RBFN (Radial Basis Function Network) has been utilizedto regulate the steady state performance of microgrid components without any fluctuations. The RBFN compares the error signal from various components including DG, PV panel, Wind Turbine, BESS, AC, and DC loads with the actual specified values to check the saturation limit of error signals. These error signal values are dynamic and are optimized using the Harmony Search (HS) Optimization Algorithm. After this, the Saturation Attentive Freezing algorithm is employed, which controls only the integration part of the PID controller. It employs restricted integration, which means that the integrator action is allowed only when the control signal from various energy sources is not saturated. When the control output reaches the saturation limit, the integrator is frozen until the system comes back within the operating range. This helps to avoid the wind-up effect by preventing the error accumulation in the integration part.The Optimized Neuro Restrictive Integration Regulator helps to control the integration process so that large overshoots of the control signal and prolonged settling times of the controller can be overcome. This helps to avoid the wind-up effect and improves the steady-state performance of the Hybrid AC/DC microgrid.

Figure 1 shows the architecture of the Bidirectional Converter with Spike Suppressed Switching and Optimized Neuro Restrictive Steady-State Controller. The circuit features a Synergic TVSD, consisting of TVS diodes on both AC and DC sides, to protect the converter from voltage spikes caused by load variations. For the purpose of preventing magnetic coupling, a Dualistic Field Decoupler is connected in parallel with the inductor and transformer. Twin Ultra-Fast Recovering Diodes (TUFRDs) and a Mid-Snubber unit are employed to allow for quicker current switching and to absorb rapid spikes in the magnetic field. The Optimised Neuro Restrictive Integration Regulator is intended to govern the steady-state functioning of various microgrid components without causing fluctuations.

2.1.1 Spike suppressed switching circuit

To reduce the switching loss in the converter during switching operation, a Spike Suppressed Switching Circuit is proposed, which utilizes Synergic TVSD and a Dualistic Field Decoupler.

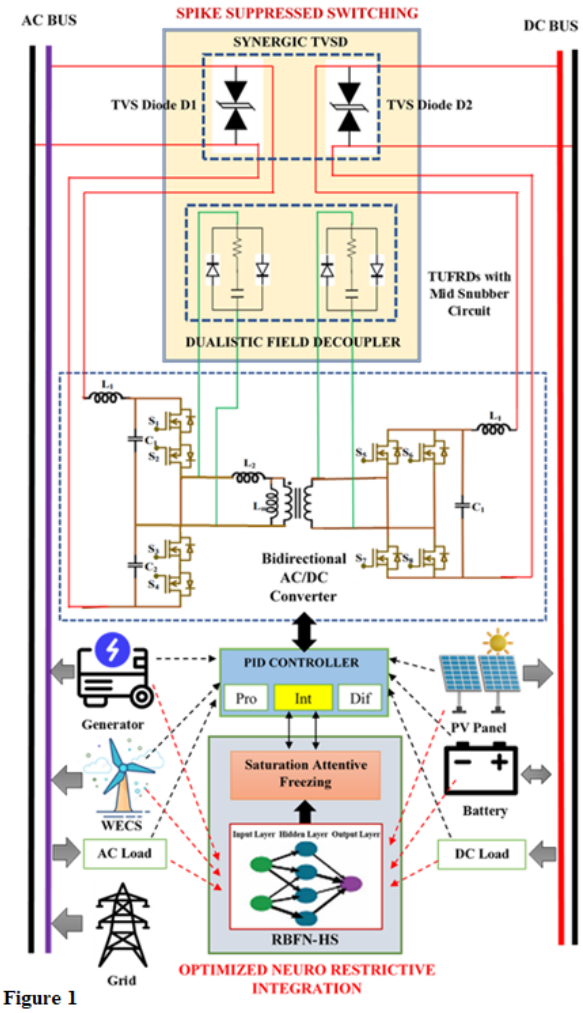

Fig. 1 — Architecture of the bidirectional converter with spike suppressed switching and optimized neuro restrictive steady-state controller.

The proposed Synergic TVSD has been introduced with two comparable TVS (Transient Voltage Suppressor) diodes with the same properties. TVS diodes are semiconductor devices that are particularly developed to deal with transient voltage spikes and safeguard electronic circuits against voltage surges. In the proposed model the two TVS diodes D_1 and D_2 are connected in parallel, which means that their anodes (one end) and cathodes (the other end) are connected in pairs. When diodes D_1 and D_2 connect in parallel, the voltage across their terminals is the same. A bi-directional model is used in the proposed method that includes two mutually opposing avalanche diodes connected in series that are capable of creating a bidirectional transient-voltage-suppression diode and are connected in parallel with the protective device. The Synergic TVSD has a convenient location on the converter's AC and DC sides. This implies that one pair of TVS diodes is coupled to the converter's AC input or output, while the other pair is connected to the converter's DC input or output. They are incorporated into the converter's electrical pathways, developing an integral component of the converter's circuits. When there is a voltage spike, the synergic TVS diodes quickly flip to a low-resistance state, enabling the transient current to pass through them. This overall process absorbs the spike's energy and lowers the voltage across the hidden components.

After this synergic TVS diode, the Dualistic Field Decoupler is designed to eliminate magnetic coupling between components like inductors and transformers to reduce energy loss and ensure efficient functioning. This decoupler comprises a Twin Ultra-Fast Recovering Diode (TUFRD) and a Mid-Snubber unit, which is also provided in parallel connection to the inductor and transformer. In order to quickly switch the current, twin ultra-fast recovering diodes (TUFRDs) are utilized, which is made possible by low junction capacitance and fast charge carrier recombination. By connecting them in parallel with the inductor and transformer, they provide an additional channel for the current passage. TUFRDs are diodes that have the unique property of having a very quick switching time. The time it takes for a diode to switch off after being forward-biased is referred to as switching time. Junction capacitance is a measure of the capacitance inherent in the internal structure of a diode and it is a crucial characteristic of diodes used in high-frequency applications. TUFRDs have a low junction capacitance. Low capacitance implies that these diodes quickly alter their voltage across the junction, which is required for fast switching. High capacitance slows down the switching process. TUFRDs start producing current when a voltage is provided in the forward bias direction. TUFRDs function as a low-resistance route for the flow of electrical current when turned on, which implies that current flows through them with low resistance. Charge carriers travel through the TUFRD from the anode to the cathode during the ON state. TUFRDs enable rapid recombination of these charge carriers when the diode is turned off. TUFRDs are suited for high-speed applications due to their fast transition from conducting to non-conducting states. TUFRDs are turned off when the voltage polarity is reversed. TUFRDs have a high impedance when turned off, essentially necessary for stopping current flow in the reverse direction.

Figure 2 shows the Spike suppressed switching circuit of the proposed model. The proposed Spike Suppressed Switching Circuit part consists of a couple of TVS diodes connected in parallel to the main buses both at the AC side and DC side, which absorb the voltage spikes. Also, the Dualistic Field Decoupler is

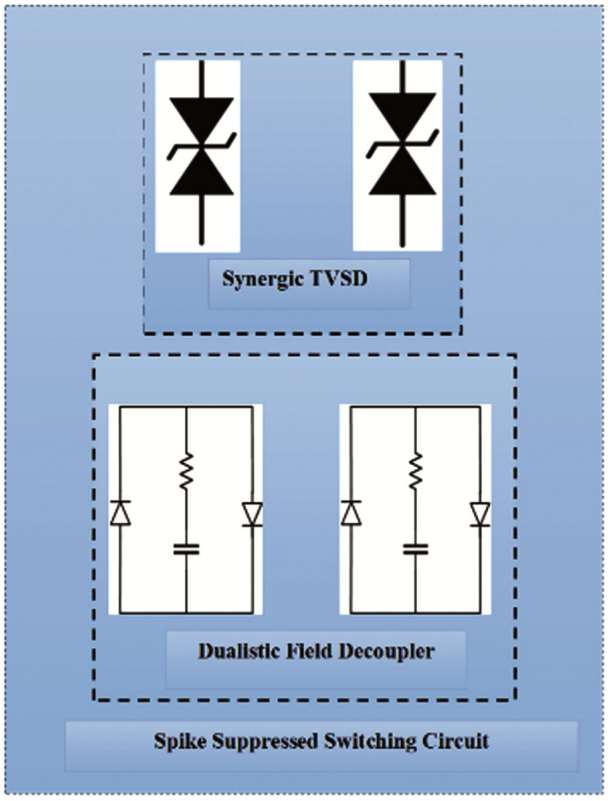

Fig. 2 — Proposed spike suppressed switching circuit.

provided in parallel connection to the inductor and transformer to avoid magnetic coupling which consists of a TUFRD and a Mid-Snubber unit. The Mid-Snubber unit contains a resistor and a capacitor connected in series and this unit is provided in a center-parallel arrangement to the TUFRDs, this capacitor provides additional protection to this proposed circuit.

The Mid-Snubber unit consists of a resistor and a capacitor linked in series, and it is coupled to the TUFRDs in a center-parallel configuration. It serves as an extra protective component by absorbing excess quick spikes in magnetic field variation induced by abrupt voltage fluctuations. The clamping of the spikes using a Mid-snubber requires computing the characteristic impedance of the resonant circuit, which is provided by the following equation (1)

$$Z = 2\pi f_x L \quad \dots (1)$$

Where Z is the impedance of the resonant circuit and L is the inductance. The capacitor is designed in such a way that its impedance at the clamping frequency is considered equal to the resistor, as demonstrated in the following equation (2):

$$C_s = \frac{1}{2\pi f_x R} \quad \dots (2)$$

When the switching frequency is f_x, R is theresistor and C_s is the capacitor of the Snubber unit. The Mid-Snubber unit's capacitor plays an essential role in absorbing the excess quantity of rapid spikes in the magnetic field variation induced by the sudden voltage spike. The capacitor begins to charge as the voltage rises. The capacitor absorbs the energy of the voltage explosion. Capacitors store energy in an electric field, and as the voltage across their plates grows, correspondingly rises the amount of energy stored. The capacitor absorbs energy, which helps to minimize the fast fluctuations in the magnetic field induced by the voltage spike. Increasing the capacitor value increases peak power while decreasing switching loss. Switching loss is one of the most significant energy losses in a converter. The switching loss (P_{loss}) is expressed in the equation (3)

$$P_{loss} = \frac{1}{12} V_c I_m \frac{1}{\pi} \int_{-\frac{\pi}{2}}^{\frac{\pi}{2}} cos\theta d\theta \quad \dots (3)$$

Where V_c is the equivalent DC voltage and $I_m$is the amplitude of the phase current.Magnetic fields around inductors and transformers are able to allow eddy currents to flow through neighboring conductive materials, resulting in energy loss and heating.

Therefore, the innovative Spike Suppressed Switching Circuit enhances switching speed, minimizes switching loss, and takes into account the parasitic effect on multiple component interaction, reducing magnetic coupling and enhancing converter performance.

2.1.2 Optimized neuro restrictive integration regulator

In the field of microgrid regulation, a novel approach named Optimized Neuro Restrictive Integration Regulator has been proposed, which includes a Restrictive Integration algorithm called Saturation Attentive Freezing, which works alongside an optimized RBFN (Radial Basis Function Network). The goal of this system is to ensure the steady-state performance of the microgrid components.

The Radial Basis Function Network (RBFN) is a type of artificial neural network used in power systems to compare the error signals generated by different components of the system, such as distributed generators (DG), photovoltaic (PV) panels, wind turbines, battery energy storage systems (BESS), alternating current (AC) loads and direct current (DC) loads. The RBFN compares these error signals with the specified values to determine whether they have reached their saturation limit. This helps maintain the stability of the power system and prevents any power failures or damage to the equipment. The RBFN consists of the input layer (*i layer*), hidden layer (*j layer*), and output layer (*k layer*).The proposed RBFN is made up of one output layer with one node and one hidden layer with a factor of nodes. The input of the hidden layer$y_i(m)$is expressed in equation (4)

$$y_i(m) = f_i\big(n_i(m)\big), i = 1 \quad \dots (4)$$

The n^{th} iteration is represented as $n_i(m) = y_i(m)$. Layer 2 is the network's hidden layer, with a membership function being a Gaussian function. When an input is fed into the network, it is changed by each radial basis function in the hidden layer before being transmitted to the output layer.The output of the hidden layer $y_j(m)$is expressed in the following equation (5)

$$y_j(m) = S\left(n_j(m)\right), j = 1,2,..,n \quad \dots (5)$$

Where $S()$ is the sigmoid function. $y_i(m)$ and $y_j(m)$ are the input and output of the hidden layer respectively. w_{ji} relates the weights of the successive hidden layers to the input layers.Layer 3 is the final result of the number of layers inside the combination

of hidden and input layers. The output layer$O_{yk}(m)$ is represented by equation (6)

$$O_{yk}(m) = f_k\big(n_k(g)\big) \quad \ldots (6)$$

Where $n_k(g) = c_z^*$, in which the control function is defined as c_z^*,and $n_k(g)$ is given in equation (7)

$$n_k(g) = \sum_j w_{kj} \times x_j(n) \quad \ldots (7)$$

Figure 3 shows the architecture of RBFN. The input layer, hidden layer, and output layer make up the RBFN. One output layer with one node and one hidden layer with a factor of nodes make up the suggested RBFN. This helps keep the power system stable and guards against equipment damage and power outages. Before an input is sent to the output layer of the network, it is altered by each radial basis function in the hidden layer. The RBFN computes the output after determining the properties of the input data using its hidden layer.The RBFN serves to guarantee the safe and steady operation of the entire system by detecting if any component is above its saturation limit by comparing the error signals with the designated values.

The proposed controller's final output from the RBFN is $O_{yk}(g)$ and w_{kj} represents the weights that connect the neurons from the hidden layer to the output layer. By assigning the right weight function to

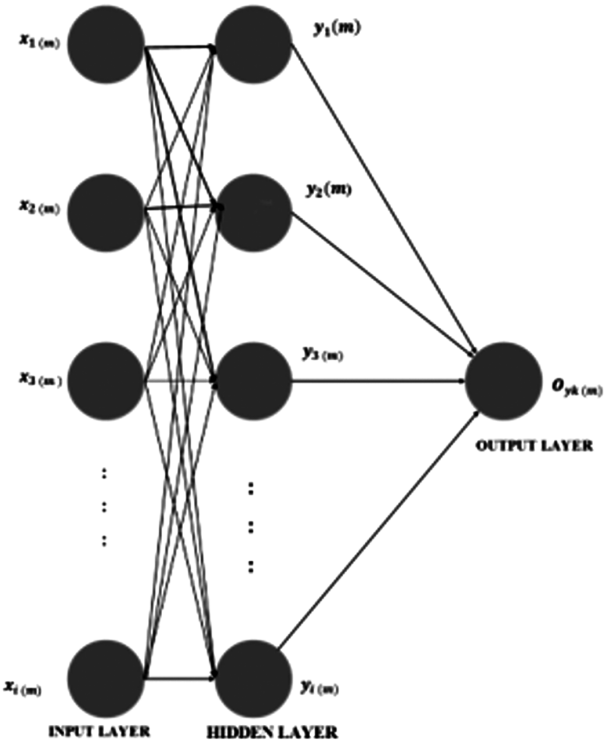

Fig. 3 — Architecture of radial basis function network

the connecting weightsw_{ji} and w_{kj}, the learning process aims to reduce the total error signal. E gives the training progress error signal, which is expressed in equation (8)

$$E = \frac{1}{2}(V_d - V_d^*) = \frac{1}{2}e^2 \quad \ldots (8)$$

Rule 1: In layer k, the weightsw_{kj} need to be changed. The widely used error signal expression is as follows in equation (9)

$$\delta_k = -\frac{dE}{dn_k} = \left[-\frac{dE}{dy_k}\frac{dy_k}{dn_k}\right] \quad \ldots (9)$$

The rationalization of weight w_{kj} is determined as in equation (10)

$$\Delta w_{kj} = -\frac{dE}{dw_{kj}} = \left[-\frac{dE}{dy_k}\frac{dy_k}{dn_k}\right]\left(\frac{dn_k}{dw_{kj}}\right) = \delta_i y_j \quad \ldots (10)$$

Then the rationalized weight is defined as in equation (11)

$$w_{kj}(m+1) = w_{kj}(m) + \xi_1 \Delta w_{kj} \quad \ldots (11)$$

Where ξ_1 denotes the layer k training rate adjustment.

Rule 2: weights of w_{ji} in layer j need to be updated. The weightw_{ji} is customized using a training program and is provided as follows in equation (12)

$$\Delta\, w_{ji} = -\frac{dE}{dw_{ji}} = \left[-\frac{dE}{dy_k}\frac{dy_k}{dn_k}\right]\left(\frac{dn_k}{dy_j}\frac{dy_j}{dw_{ji}}\right) \quad \ldots (12)$$

The connecting weight w_{ji} is updated, which is expressed in the following equation (13)

$$w_{ji}\,(m+1) = w_{ji}\,(m) + \xi_2 \Delta w_{ji} \quad \ldots (13)$$

Where, ξ_2 denotes the layer j training rate adjustment and the learning algorithm calculates error signal$E$ until the performance target is met. The RBFN uses its hidden layer to identify the characteristics of the input data and then calculates the output. By comparing the error signals with the specified values, the RBFN detects if any component is exceeding its saturation limit, which helps to ensure the safe and stable performance of the entire system.

The error signal readings are dynamic, which means they change all the time. As a result, the Harmony Search (HS) Optimisation Algorithm is employed in the proposed model to optimize these error signals. The HS algorithm is a metaheuristic optimization approach inspired by the musical practice of attempting to achieve perfect harmony. The first step of this algorithm is the initialization of the parameters. This step involves the specification of the HSA parameters, which comprise the harmony memory size (HMS), harmony memory considering

rate (HMCR), pitch adjusting rate (PAR), and the number of improvisations (NI) serving as the stopping criterion. The harmony memory (HM) is a memory location that stores all the solution vectors, representing sets of decision variables. The HMS determines the number of solution vectors in the HM. The HMCR specifies the probability of selecting a value from the HM, while the PAR regulates the degree of pitch adjustment. NI determines the number of times the algorithm runs before ending. Thus, these parameters are key to the success of the proposed HS algorithm.

The second step is the initialization of the harmony memory.HM is a storage memory that contains all possible optimization process solutions. The initial HM includes the number of randomly generated solutions to the under-study optimization issue. The initial HMx_i^j is calculated by employing a uniform distribution in the range of (U_i,L_i) is expressed in equation (14)

$$x_i^j = L_i + rand() \times (U_i - L_i) \quad \dots (14)$$

Where $(i < j < n), (i = 1,2, \dots, HMS)$ and $U(0,1)$. For n parameter obtained from this optimization process, the HM has a size of HMS, which is expressed as in the equation (15)

$$HM = \begin{bmatrix} x_{1,1} & x_{1,2} & \dots x_{1,n} \\ x_{2,1} & x_{2,2} & \dots x_{2,n} \\ . & . & \dots\dots \\ . & . & \dots\dots \\ x_{HMS,1} & x_{HMS,2} & \dots x_{HMS,n} \end{bmatrix} \quad \dots (15)$$

Where, $\begin{bmatrix} x_1^j & x_2^j & \dots & x_n^j \end{bmatrix}$ is a solution set. The third step is to compute the fitness function of all HM solutions. The fitness function for all components in the HM is determined at this stage. The fitness function values are saved in a matrix $fit(x_i \ :)$ shown in equation (15), where i=1,2,…HMS after they have been calculated.Primarily a new random number $r_1 \in (0,1)$ is produced. It is then compared to the HMCR. If $r_1 < HMCR$, each component of the new harmony is picked at random from the HM components according to equation (16)

$$x_j^{new} = x_j^a \quad \dots (16)$$

Where $j = 1,2, \dots, N$, and x^a is a random harmony vector from HM.A novel random number, $r_2 \in (0,1)$, is generated. The fine-tuning of the HMCR step component is contingent upon the value of $r_2 < PAR$. Specifically, the fine-tuning process is conducted by utilizing bandwidth B, which is defined in the following equation (17)

$$x_j^{new} = \begin{cases} x_j^{new} \pm rand() \times B & if\ r_2 < PAR \\ x_j^{new} & otherwise \end{cases} \quad \dots (17)$$

In instances where a component fails to meet the selection criteria for the HMCR, it is substituted with a value generated at random from the search box. This approach ensures that the component's absence does not impede the overall search process, as a suitable replacement is generated in its place. The New Harmony is expressed in the following equation (18)

$$x_j^{new} = L_j + \left(U_j - L_j\right) * rand[0,1] \quad \dots (18)$$

Where L_j is the lower limit and $U_j$is the upper limit of the layer j. If the fitness value of the new harmony (x_j^{new}) is greater than the fitness value of the worst harmony (x_j^{worst}) in HM, the new harmony will replace the worst harmony.Based on the present error signals, the newly created solutions are assessed using the fitness function. This assessment determines how well each new solution works in terms of error reduction and system performance. If a new solution is discovered to be superior to the present collection of solutions (Harmony Memory), it replaces the worst solution. The algorithm preserves and expands on the most successful control actions or parameter settings by updating the Harmony Memory with improved solutions. Based on the dynamic error signals, the HS algorithm continues to repeat, creating and assessing new solutions and updating the Harmony Memory. The iterative procedure enables the algorithm to react to changes in the error signals and make real-time corrections. The algorithm runs until an end requirement is reached. A specified number of iterations, a threshold degree of error reduction, or other convergence criteria are possibly used as the stopping condition. The proposed RBFN is an advanced machine learning model that helps in identifying the saturation limit of error signals for different components. The HS optimization algorithm is used to optimize these dynamic error signals, ensuring that they are always performing at their best.

Following that, the proposed Saturation Attentive Freezing method is used. The integral component of a PID controller in a control system collects the error signal over time and integrates it to move the control signal toward the desired set point. The integral action, in mathematical words, is the integration of the error signal with respect to time is represented in the following equation (19)

$$I(t) = \int_0^t e(\tau)\, d\tau \quad \ldots (19)$$

Where $I(t)$ represents the integral term at time *t*, $e(\tau)$ represents the error signal at time *t*, and $\int_0^t$ represents the integral across time.The integral component is essential for systems that have inherent biases or are vulnerable to fluctuations. Also, it is essential to remove any steady-state error that exists despite the proportional control action. It constantly modifies the control input based on an overall count of previous mistakes. When the control signal saturates (reaches its upper or lower limits), the integrator continues to collect errors, possibly resulting in substantial overshoot and instability when the control signal ultimately recovers. The SAF algorithm continually checks the control signal and identifies saturation limits. The control signal is denoted as u, the response signal is y, and the set point is y_{sp}.Following the initial set point change, the control signal (u) ascends to its upper limit of u_{max}. This control signal is not strong enough to eliminate control errors.

When u moves toward saturation, the integrator value $\eta$is frozen. Which is expressed in the following equation (20)

$$\eta = \begin{cases} 0 \; u \neq u_{max} & \& \quad e.(u - u_{max}) > 0 \\ e & otherwise \end{cases} \quad \ldots (20)$$

Where the new error is denoted as e. The SAF algorithm "freezes" the integrator when it senses that the control signal has reached its saturation limit. This signifies that the integrator's error accumulation is briefly halted or significantly slowed. Which is expressed in the following equation (21)

$$\eta = \begin{cases} 0 & u \neq u_{max} \\ e & otherwise \end{cases} \quad \ldots (21)$$

The integrator fails to produce new errors while it is frozen. This avoids additional error build-up while the control signal is saturated. To limit the influence of integrator windup, turn off the integration when the absolute value of the error signal exceeds a certain threshold. This outcome is obtained by setting the integrator input to zero during periods of high inaccuracy. In addition to enhancing controller responsiveness in the presence of actuator saturation, this strategy can minimize overshoot in instances when the system response is linear. The integral term causes a substantial overrun in the PID controller response for a linear plant. The addition of integrator windup reduction to the controller is going to significantly reduce the overshoot in that situation. The integrator wind-up avoidance is expressed in the following equation (22)

$$u = K_p \left(e + K_i \int_0^t qe\, d\tau + K_d \frac{de}{dt} \right) \quad \ldots (22)$$

Where $K_p$is the gain K_i is the integral term and $K_d$is the derivative term. The approach prevents additional error accumulation in the controller's integration section by freezing the integrator during saturation. Enabling the integrator to continue collecting errors during saturation is going to exacerbate the wind-up effect. A controlled integration is considered with this Optimised Neuro Restrictive Integration Regulator to overcome the large overshoot of the control signal and the prolonged settling time of the controller, avoiding the wind-up effect and improving the steady state performance of the Hybrid AC/DC microgrid.

Overall, with this proposed controlling approach, the parasitic effect on multiple component interaction has been considered to eliminate switching losses, and controlled integration of errors is considered to improve the steady-state performance of the Hybrid Microgrid.

3 Results and Discussion

This part includes a comparison section to make sure the proposed system functions effectively and a full discussion of the implementation results and performance.

3.1 Experimental setup

The simulation results are discussed below. This work has been implemented in the MATLAB working platform using the following system specifications.
Software: MATLAB
OS: Windows 10 (64-bit)
Processor: Intel i5
RAM: 8GB RAM

3.2 Simulated output of the proposed model

This section interprets and analyses a simulation output of the proposed Bidirectional Converter with Spike Suppressed Switching and Optimized Neuro Restrictive Steady-State Controller model.

Figure 4 illustrates the proposed microgrid's bidirectional hybrid AC/DC converter. A Spike Suppressed Switching Circuit portion of this proposed bidirectional hybrid AC/DC converter comprises a couple of TVS diodes linked a couple of TVS diodes linked in parallel to the main buses on both the AC and DC sides. The Dualistic Field Decoupler, which

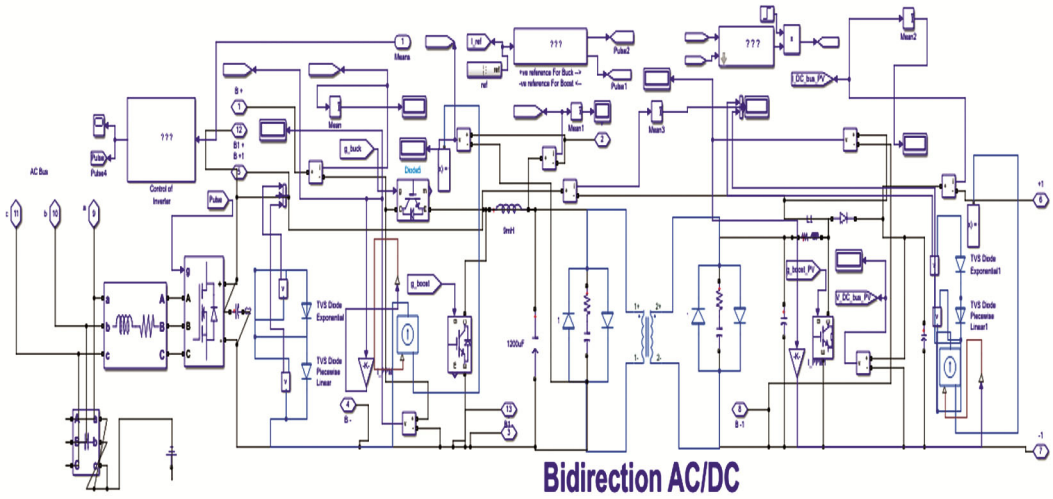

Fig. 4 — The proposed bidirectional hybrid AC/DC conveter.

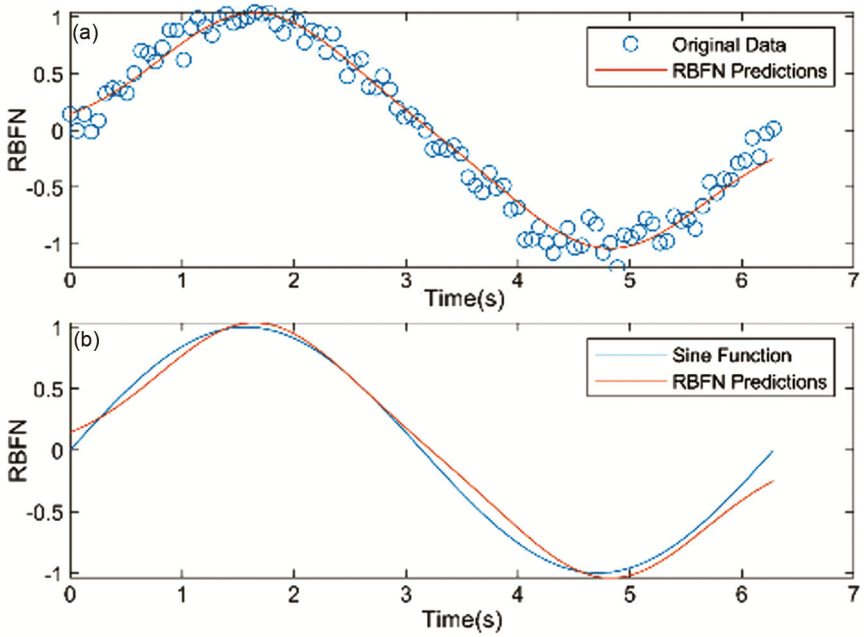

Fig. 5 — RBFN prediction of the proposed model.

comprises a Twin Ultra-Fast Recovering Diode and a Mid-Snubber unit, is also provided in parallel connection to the inductor and transformer to eliminate magnetic coupling. The Mid-Snubber unit is linked in series with the TUFRDs and consists of a resistor and a capacitor.

Figure 5 shows the RBFN prediction of the proposed model. From the figure the circle shows the original data and the second part of the figure the red waveform is the RBFN predicted output of the proposed model. The RBFN monitors and predicts error signals to ensure that the system responds correctly to departures from the expected reference values. The amplitude of the sine function and RBFN predictions waveform ranges from -1 to 1.

3.3 Performances metrics of the proposed system

The Performance metrics of the proposed Bidirectional Converter with Spike Suppressed Switching and Optimized Neuro Restrictive Steady-State Controller and the achieved outcome were explained in detail in this section.

Figure 6 shows the Output voltage and current of the proposed hybrid AC/DC converter. The period of

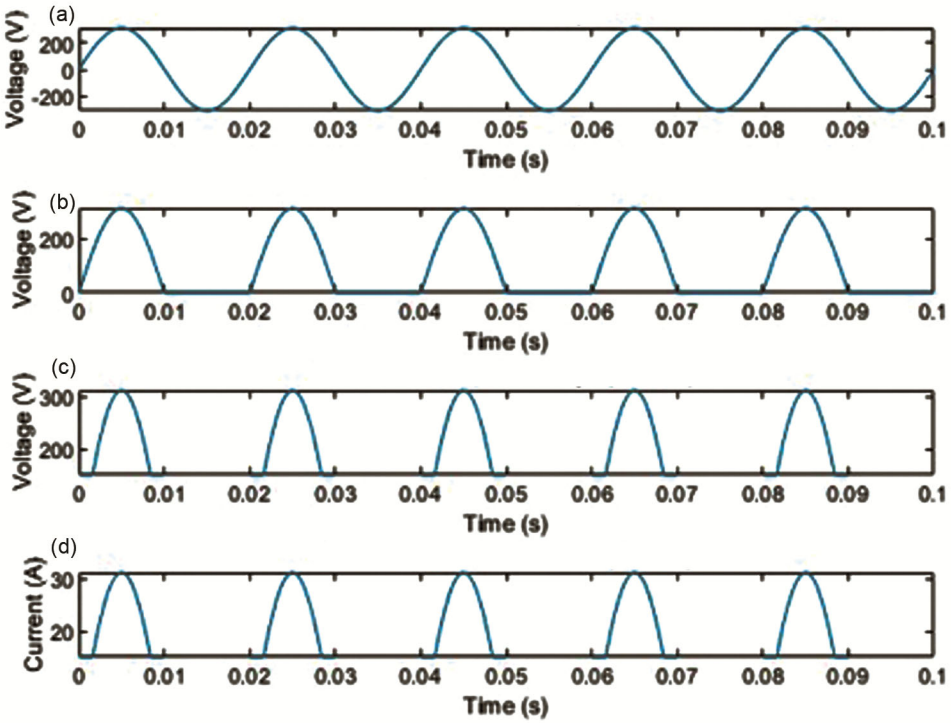

Fig. 6 — Output voltage and current of the proposed AC/DC converter.

the AC input voltage sine waveform, which is the length of time it takes to complete one full cycle, ranges from 0 to 0.02s, and the voltage ranges from -300 to 300V. The converter rectifies the input AC voltage to generate a DC output voltage while converting AC to DC. The pulsing waveform of the output voltage going to look similar to the positive half of the input AC sine wave. From time 0 to 0.01s it generates one positive half cycle and the voltage ranges from 150 to 300V. The converter output current ranges from 15 to 30 A.

Figure 7 shows the battery state of charge over time performance of the proposed model. The Optimised Neuro Restrictive Integration Regulator guarantees that battery control signals are optimized and are free from significant overshoots or wind-up effects. This implies that the battery is handled more effectively, lowering the chances of overcharging or undercharging and ensuring a more constant level of charge over time. When time increases the battery SoC also increases. The proposed model attains a maximum battery SoC value of 9.5 when the time is 10 hours.

Figure 8 shows the magnetic coupling before and after decoupler of the proposed model. In the blue line shows the output before decoupler and red shows after decoupling of the proposed model. Voltage

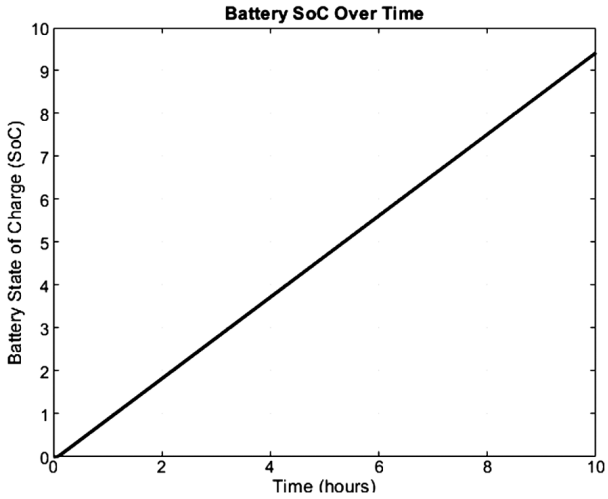

Fig. 7 — Battery state of charge (SoC) over time of the proposed model.

variations in the microgrid might show abnormalities owing to magnetic coupling effects before applying the Dualistic Field Decoupler. TUFRD is a Dualistic Field Decoupler component that has low junction capacitance and enables faster charge carrier recombination. It allows for quicker switching of current flow in opposite directions. This helps to mitigate the effects of magnetic coupling. After applying to decoupler, the impact of magnetic

coupling on voltage fluctuations is considerably reduced and ranges from -1.05V to 1.05V.

Figure 9 shows the wave form plot of switching pulse with and without circuit. Synergic TVSD actively reduces voltage spikes induced by transient currents via the Spike Suppressed Circuit. As a result, the voltage waveform is reasonably consistent and free from huge spikes. The figure shows a voltage curve that is reasonably flat and steady over time. The voltage begins to shift from 0 V to 10.5 V, during the switching event. When sudden transient currents or load changes occur, the voltage waveform may produce spikes and overshoots in the absence of the switching circuit. These spikes include the potential to harm the converter circuit's protected components. In this condition, at time 0.5 the voltage suddenly increased from 0 V to 10.5 V.

Figure 10 shows the switching loss of the proposed model. The switching loss per cycle becomes large at high switching frequency. This is because each cycle has a large number of sudden switching events, resulting in increased energy dissipation owing to switching losses. The Synergic TVSD and Dualistic Field Decoupler are crucial in this case because they actively suppress voltage spikes, and decrease switching losses to make them manageable. At a

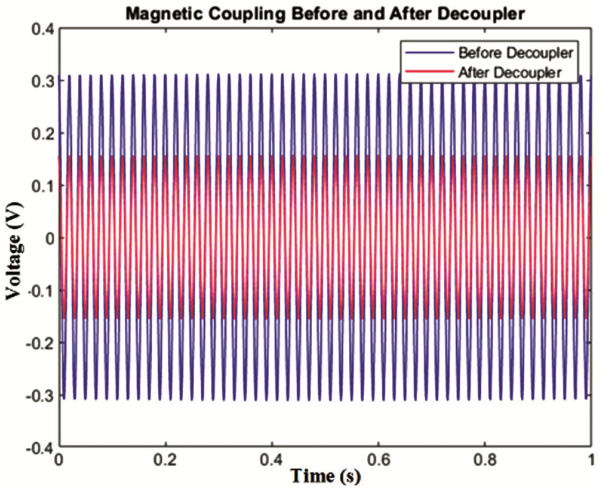

Fig. 8 — Magnetic coupling of the proposed model.

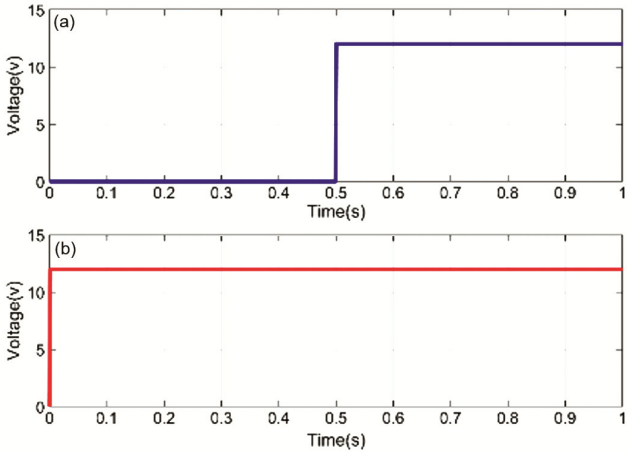

Fig. 9 — Wave form plot of switching pulse with and without circuit.

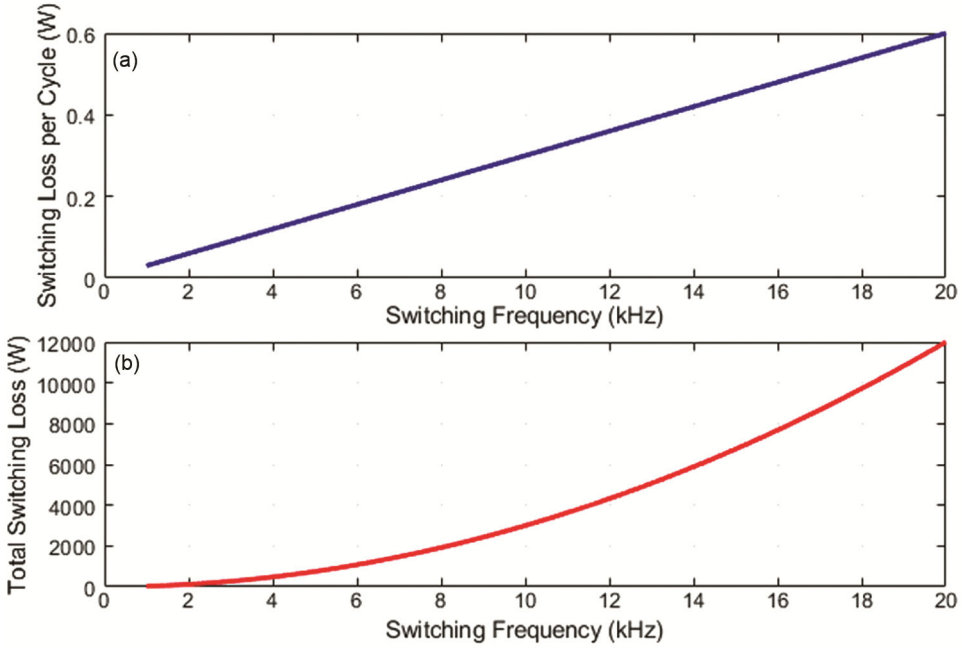

Fig. 10 — Switching loss of the proposed model.

frequency of 20KHz the proposed model attains a total switching loss of 12000W, and a switching loss per cycle value of 0.6W.

3.4 Comparative analysis of the proposed model

This section highlights the proposed method's performance by comparing it to the outcomes of existing approaches such asgenetic algorithm (GA)[28], Improved Particle Swarm Optimization (IPSO)[28], Ant-Lion Optimizer algorithm with Recurrent Neural Network (ALORNN)[28], Common Scrambling Algorithm (CSA)[28], Hybrid Crow Search with Radial Basis Function Neural Network (HCS-RBFNN)[28], Radial Basis Functions (RBF)[26], Broad Learning System (BLS)[26], Bacterial foraging optimized Extreme Learning Machine (BFO-ELM)[26], and shark smell optimization-Broad Learning System (SSO-BLS)[27] showing their results based on various metrics.

Figure 11 shows the comparison of switching loss of the proposed model. Existing algorithms such as GA, IPSO, ALORNN, CSA, and HCS-RBFNN has a switching loss of 0.75W, 1.0W, 1.75W, 3.5W and 0.2%. Compared with existing models the proposed model has a low switching loss. The proposed model attains a low switching loss value of 0.15W.

Figure 12 shows the comparison of the converter efficiency of the proposed model with various existing models. Existing models such as GA, IPSO, ALORNN, CSA, and HCS-RBFNN have a converter efficiency of 88%, 89%, 91%, 93%, and 98%. The proposed model has a converter efficiency of 99%. Compared with existing models the proposed model achieves a high converter efficiency value.

Figure 13 shows the comparison of the power of the proposed model with existing models. The existing models such as Base, ALORNN, CSA, and HCS-RBFNN attains a power value of 1700W, 1750W, 1850W, and 1900W. The proposed model achieves a high power value of 1950W. Compared with existing models the proposed model attains a high power value.

Figure 14 shows the comparison of error of the proposed model with existing models. Existing models such as RBF, BLS, BFO-ELM, and SSO-BLS attains an error value of 0.33%, 0.12%, 0.07% and 0.04%. The proposed model achieves an error value of 0.03%. Compared with existing models the proposed model attains a minimum error value.

Figure 15 shows the conduction loss of the proposed model with existing models. Existing

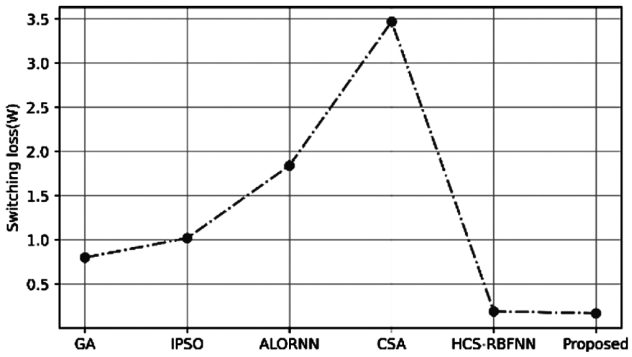

Fig. 11 — Comparison of switching loss.

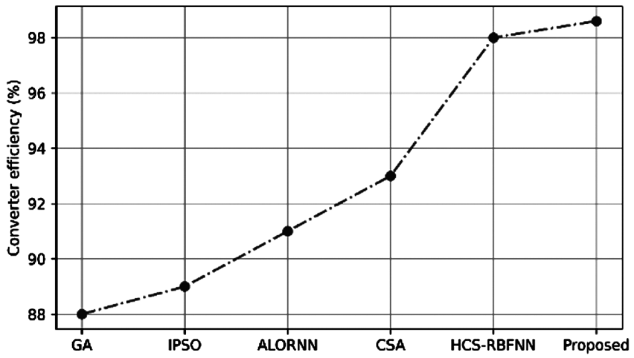

Fig. 12 — Comparison of converter efficiency.

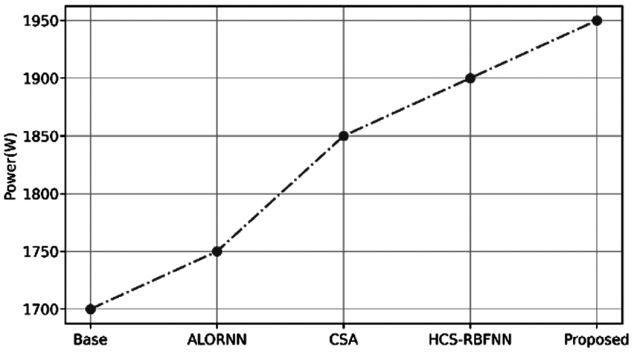

Fig. 13 — Comparison of power.

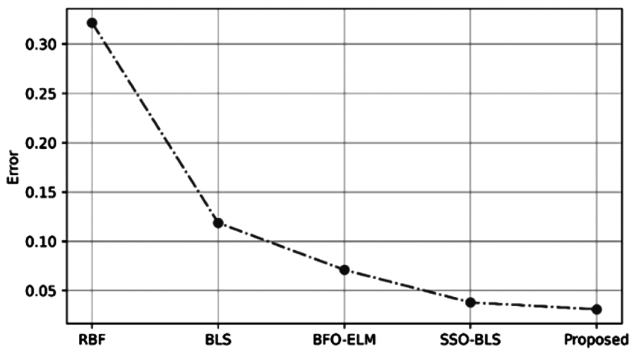

Fig. 14 — Comparison of error.

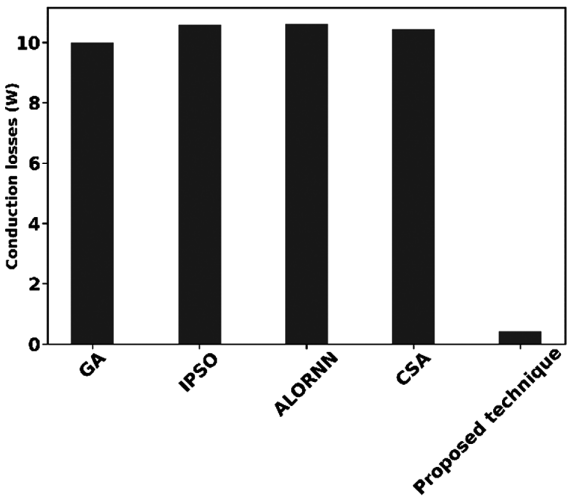

Fig. 15 — Comparison of conduction loss.

models such as GA, IPSO, ALORNN and CSA has a conduction loss of 10W, 11W, 10.8W and 10.2W. Compared with exoisting models the proposed model has a low conduction loss. The proposed model has a high 0.5W.

Overall the proposed model shows that it is more efficient and more accurate when compared to previous models such as GA, IPSO, ALORNN, CSA, and HCS-RBFNN. The proposed model attains a maximum battery SoC value of 9.5 and a switching loss per cycle value of 0.6W. This proposed model achieves an error value of 0.03% when compared to existing techniques like RBF, BLS, BFO-ELM, and SSO-BLS. This proves that the proposed system performed well when compared to other existing techniques

4 Conclusion

A novel Bidirectional Converter with Spike Suppressed Switching and Optimized Neuro Restrictive Steady-State Controller is proposed to reduce the switching loss and improve the steady-state performance. In order to reduce the switching loss in the converter Spike Suppressed Switching Circuit has been introduced, in which Synergic TVSD is utilized to avoid excessive voltage caused by external load fluctuations and a Dualistic Field Decoupler provided a parallel connection to the inductor and transformer to overcome the magnetic coupling. A new Optimised Neuro Restrictive Integration Regulator is proposed, which uses a Saturation Attentive Freezing algorithm and optimised RBFN to regulate the stable state performance of microgrid components without oscillations. The proposed model attains a high battery SoC value of 9.6 and a total switching loss per cycle value of 0.6W. Compared with existing models the proposed model achieves a high power value of 1950W, a converter efficiency of 99%, and a low switching loss of 0.15W. Thus, the proposed model was utilized to provide a better performance and reduce switching loss according to the results.This shows that the proposed approach outperformed other existing methods.

References

1 Mamatha S, & Mallesham G, *In Recent Developments in Electrical and Electronics Engineering: Select Proceedings of ICRDEEE* 2022,277-289. *Singapore: Springer Nature Singapore,* (2023).

2 Shen X, Shuai Z, Huang W, Shen C, Shen Y, & Shen Z J, *CSEE J Power Energy Systems,* (2022).

3 Al-Gaheeshi A M R, Rashid F L, Eleiwi M A, & Basem A, *Int J Heat Technol*, 41 (2023) 3.

4 Eldoromi M, Birjandi AAM, & Dehkordi NM, *In 2023 14th Power Electronics, Drive Systems, and Technologies Conference (PEDSTC),*(2023 January)1-5. *IEEE.*

5 Sarwar S, Kirli D, Merlin MM, & Kiprakis AE, *A Review. Energies,* 15(23) (2022) 8851.0

6 Neto AOC, Soares AL, Barbosa VF, Rodrigues DB, Freitas LC, & De Lima GB, *IEEE J Emerging Selected Topics in Power Electronics,* (2023).

7 Aryani DR, Adi FS, Kim JS, & Song H, *Energy Reports*, 8 (2022)520-531.

8 Nallolla CA, PV, Chittathuru D, & Padmanaban S, *A Comprehensive Review. Electronics,* 12(4) (2023)1062.

9 Bharatee A, Ray PK,Subudhi B,& Ghosh A, *A Review. Energies,* 15(19) (2022) 7176.

10 Mansour HB, Chaarabi L, Jelassi K, & Guerrero JM, *IJCSNS,* 22(3) (2022) 355.

11 Jeyaraj PR, Asokan SP, & Karthiresan AC, *Electric Power Systems Research,* 205 (2022)107730.

12 Awais M, Khan L, Khan SG, & Awaisand Jamil M, *Energies,* 16(4) (2023)1902.

13 Çimen H, Bazmohammadi N, Lashab A, Terriche Y, Vasquez JC, & Guerrero JM, *Appl Energy,* 307 (2022) 118136.

14 Jasim AM, Jasim BH,Neagu BC, & Alhasnawi BN, *Electronics,* 12(1) (2022) 187.

15 Akpolat AN, Dursun E, & Kuzucuoğlu AE, *IEEE Access,* 9 (2021) 106641.

16 Silveira JPC, dos Santos Neto PJ, Moura BC, Ruppert Filho E, & dos Santos Barros TA, *Energy Reports,* 9 (2023) 1743.

17 Ortiz L, Orizondo R, Águila A, González JW, López GJ, & Isaac I, *Heliyon,* 5(12) (2019).

18 Yu H, Niu S, Shao Z,& Jian L, *Int J Electrical Power Energy Systems,* 135 (2022) 107476.

19 Roy TK, & Mahmud MA, *Cleaner Energy Systems,* 3 (2022) 100044.

20 Kim TG, Lee H, An CG, Yi J, & Won CY, *Energies,* 16(4) (2023) 1787.

21 Jasim AM, Jasim BH, Bureš V, & Mikulecký P, *IEEE Access,* 11 (2023) 2164.

22 Lv Z, Zhang Y, Xia Y, & Wei W, *IET Generation, Transmission Distribution,* 14(17) (2020) 3594.

23 Bandla KC, Gururaj MV, and Padhy NP, *In 2020 IEEE International Conference on Power Electronics, Smart Grid and Renewable Energy (PESGRE2020),* (2020 January)1-6. IEEE.

24 Abulanwar S, Ghanem A, Rizk ME, & Hu W, *Appl Energy,* 304 (2021)117756.

25 Yang P, Shang Z, Liu C, Peng Y, Zhu Z, & Chen Z, *CSEE J Power Energy Systems,* 6(2) (2020) 291.

26 Reddy PY, & Saikia LC, *Syst Sci Control Eng,* 11(1) (2023) 2188406.

27 Wang L, &Xue A, *Energies,* 14(23) (2021) 7911.

28 Rajasekaran R, & Rani P U, *Appl Soft Comput,* 99 (2021) 106901.